communications materials

Article

https://doi.org/10.1038/s43246-025-00746-x

Electrically chargeable inorganic persistent luminescence in an alternating current driven electroluminescent device

Check for updates

Cunjian Lin[1,2,7], Rujun Yang[3,7], Zishuang Wu[4], Yajing Wang[3], Chenhan Zhan[3], Hirohisa Miyata[1], Xiankan Zeng[2], Yuantian Zheng[3], Shihai You[2] ✉, Ying Lv[5] ✉, Yixi Zhuang[3], Rong-Jun Xie[3,6] & Jumpei Ueda[1] ✉

Persistent luminescence (PersL) in inorganic materials, lasting from seconds to even days, has attracted considerable attention. Despite the promise of electric power-driven PersL for lighting and display device applications due to its convenience and manageability, studies on electrically driven inorganic PersL are lacking. Here, we report an inorganic PersL in electroluminescent devices, which shows an energy storage effect that persists beyond 24 h after charging with an alternating current electric field at 250 K. The spin-coating method-prepared emission layer composites consist of a small bandgap copper-doped zinc sulfide core, a high dielectric constant alumina shell and a chemically passivated dielectric polydimethylsiloxane medium (ZnS:Cu@AlO_x@PDMS), and these composites exhibit well-distributed electric fields and excellent operational stability. Thermoluminescence characterization reveal that PersL with an ~ 0.3 eV trap depth in electroluminescent devices mainly arises from the charge separation via hot-electron impact excitation and charge trapping within trap states in the emission layer. This study on electrically chargeable PersL in alternating current-driven electroluminescent devices can enhance our understanding of luminescence mechanisms in inorganic semiconductors.

Persistent luminescence (PersL) materials are capable of storing photon energy in trap states and delaying light emission for several seconds to hours after excitation and have motivated ongoing explorations of their better performance in many advanced applications, such as information storage, alternating-current driven light-emitting diodes (AC-LEDs), bioimaging and sensing[1–6]. Through the continuous effort of researchers, a variety of PersL materials with appealing properties have been successfully created in both inorganic and organic systems[7–10]. Generally, PersL can be described as an electron trapping-detrapping process, as shown in Fig. 1a, b[11]. This process begins with band-to-band excitation, where electrons are directly excited from the valence band (VB) to the conduction band (CB) of host materials and then partially captured by traps. After ceasing excitation, the trapped charge carriers can escape from the traps under external stimuli such as thermal activation or near-infrared stimulation and return to CB; finally, these charge carriers recombine with holes in the luminescence centers to produce PersL. However, most reported PersL materials, especially inorganic phosphors, can only be subjected to photoexcitation. Therefore, their application is limited in lighting and display devices, and this deficiency motivated our research for the attainment electro-excited PersL[12,13]. For instance, electrically excitable PersL not only addresses flicker problems but also facilitates device miniaturization and integration by eliminating the need for an additional inorganic phosphor layer in AC-LEDs[14,15]. In this context, developing PersL materials that can be electrically excited is highly important for extending their applications in optoelectronic devices.

This motivation has resulted in great efforts in exploring electrically excitable PersL materials, and significant advances have been achieved in organic PersL compounds. For example, a series of organic light-emitting

[1]Graduate School of Advanced Science and Technology, Japan Advanced Institute of Science and Technology, Nomi, 923-1292, Japan. [2]Research Institute of Frontier Science, Southwest Jiaotong University, Chengdu, 610031, China. [3]College of Materials, and Fujian Key Laboratory of Surface and Interface Engineering for High Performance Materials, Xiamen University, Xiamen, 361005, China. [4]Institute of Flexible Electronics (IFE, Future Technologies), Xiamen University, Xiamen, 361005, China. [5]Nanchang Key Laboratory of Photoelectric Conversion and Energy Storage Materials, College of Science, Nanchang Institute of Technology, Nanchang, 330099, China. [6]State Key Laboratory of Physical Chemistry of Solid Surfaces, Xiamen University, Xiamen, 361005, China. [7]These authors contributed equally: Cunjian Lin, Rujun Yang. ✉e-mail: shihai.you@swjtu.edu.cn; yinglv@nit.edu.cn; ueda-j@jaist.ac.jp

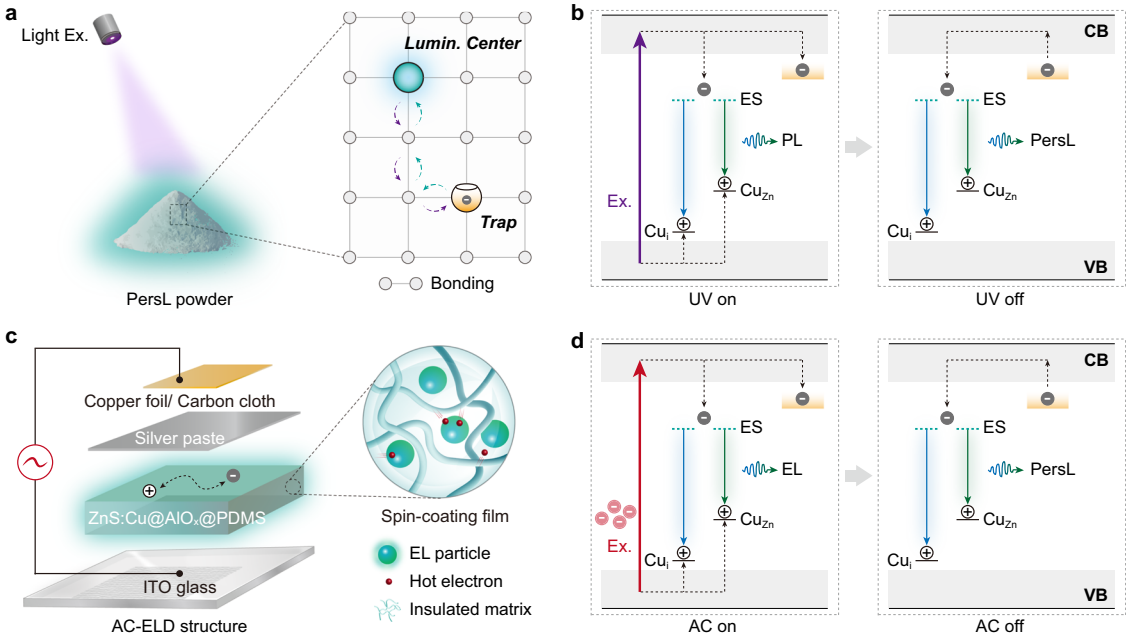

Fig. 1 | Schematic diagram of the PersL under light irradiation and AC charging. **a** Diagram of PersL powder under optical excitation. **b** PersL mechanism with light excitation on and off. Under optical excitation, the radiative transition of electrons results in PL. Partial holes and electrons are captured by the luminescent center and trap, respectively. The trapped charge carriers escape and subsequently recombine at the luminescent center to obtain the PersL. **c** Structure of AC-ELD. **d** Proposed PersL mechanism with electrical charging on and off. Under AC excitation, the electrons in the VB are excited by the AC-generated hot electrons, resulting in EL. Similar to optically excited PersL, some carriers are separated and trapped in the trap state. PersL appears after the combination of holes and electrons in the luminescent center. Abbreviations and labels: light excitation (purple line), hot electron and related excitation (red balls and line), luminescent centers: interstitial Cu_i (blue-Cu) and substitutional Cu_{Zn} (green-Cu), excited state (ES, cyan dotted line), trap state (orange line), electron (gray ball), and hole (white ball).

diodes (OLEDs) have been successfully assembled by incorporating organic room-temperature phosphorescence (RTP) emitters, thermally activated delayed fluorescence (TADF) dimmers, or long-persistence luminescence (LPL) compounds as electroluminescent layers to achieve intriguing electro-excited PersL performance[16–19]. Despite these impressive breakthroughs, the practical applications of these organic materials are still significantly limited by their relatively short lifetime (i.e., several seconds) and their sensitivity to environmental moisture and oxygen, necessitating the use of encapsulation techniques or an inert gas atmosphere[20,21]. In addition, these OLEDs are driven by direct current (DC), which causes serious charge accumulation problems as well as significant energy loss when connected to generally available AC power sources (i.e., 110/220 V, 50/60 Hz)[22]. Compared with their organic counterparts, inorganic PersL phosphors usually have a longer duration and superior environmental stability; thus, they are highly promising candidates for electroluminescent devices (ELDs) to attain outstanding PersL. However, no studies have been reported on electrically driven PersL in inorganic phosphors. Therefore, attaining an electrically excitable PersL in inorganic phosphors and understanding its corresponding underlying electron behaviors are crucial for their future application in optoelectronic devices.

Herein, we report the fabrication of an electro-excited PersL in an inorganic zinc sulfide (ZnS) phosphor within an AC-driven ELD structure (Fig. 1c). AC-driven ELDs, with frequent reversal of the electric field, effectively prevent charge accumulation and improve power efficiency[22]. A metal-doped ZnS PersL phosphor (ZnS:Cu) with a small bandgap was coated with high dielectric constant aluminum oxide (AlO_x), increasing the probability of hot-electron impact band-to-band excitation, thereby promoting efficient carrier separation, and electron and hole capture by crystalline defects and Cu^+, respectively (Fig. 1d)[23,24]. The phosphor@polydimethylsiloxane (PDMS) ultrathin dielectric layer (~100 μm), fabricated through a spin coating method, enables precise electric field distribution around particles and effectively inhibits direct current injection and electrochemical reactions. The thermoluminescence (TL) measurements were conducted on ZnS@AlOx@PDMS-based ELDs after electrical charging to assess the generated traps and trap depth, which were found to be comparable to those of the same EML materials after light irradiation. The fabricated ELDs exhibit minute-level PersL, temperature-dependent decay characteristics, and hour-level energy storage effects within the EML, thus facilitating applications such as medical identification labels.

Results and discussion

Photophysical properties of ZnS:Cu@AlO_x phosphor

To validate our hypothesis, we selected the ZnS:Cu@AlO_x PersL complex as a typical example, among which ZnS:Cu and AlO_x served as a PersL core and a high dielectric constant shell, respectively[25]. The X-ray diffraction (XRD) patterns show that the ZnS:Cu powders contain both cubic and hexagonal phases, and the substitution of Cu^+ and coating with AlO_x have no impact on the phase purity (Fig. 2a). Energy dispersive X-ray (EDX) spectroscopy mappings reveal a uniform distribution of Al and O on the particles (Fig. 2b). The average particle size is determined to be approximately 22.5 μm by randomly collecting 161 particles (Fig. 2c). The smaller particle size facilitated the formation of a dense and smooth doped thin ZnS:Cu@AlO_x@PDMS film (Fig. 2d i). The thin film thickness is influenced by the spin coating rate, demonstrating a thinning trend at higher rotational speeds (Supplementary Fig. 1). Nevertheless, doping more semiconductor powders in the thinnest possible layer was advantageous for enhancing the EL and PersL brightness of the device. An optimized speed of 500 rpm was used to achieve a film thickness of approximately 124.2 μm according to the alternating current (AC) charging PersL decay duration (Fig. 2d ii and Supplementary Fig. 2).

To evaluate the optical properties of the complex in AC electroluminescent devices (ELDs), we subsequently conducted high-resolution vacuum ultraviolet (VUV) spectroscopy (150–400 nm) on the ZnS:Cu@AlO_x phosphor. (Fig. 2e). The host excitation energy at 10 K was estimated to be 3.82 eV (at ~325 nm); this was further adjusted by

multiplying it by 1.08 to incorporate the electron-hole binding energy, and a final value of 4.12 eV was obtained (Fig. 2e ii)[26]. AC charging readily generates hot electrons with energy equal to or exceeding the ZnS band gap[23]. Numerous studies have reported blue and green emissions from copper-activated ZnS phosphors, yet the nature of the key emission process is debatable[27–32]. We ascribe the luminescent centers of the two typical photoluminescence (PL) peaks at approximately 450 and 515 nm to interstitial Cu_i and substitutional Cu_{Zn}, respectively (Fig. 2e iii)[33,34]. The associated excited state scenario is highly complex, involving factors such as CB, sulfide vacancy (V_s), and substitutional Al_{Zn}; therefore, we refrain from providing clear deductions here. Compared to blue light, green light exhibits a longer lifetime of 0.56 ms at 0.17 ms under UV excitation (Fig. 2f).

Electrically driven PersL properties of ELD

Subsequently, we determined the PersL duration of ELDs under various electrical field excitation conditions. First, varying stimulation times did not result in significant differences; here, we selected a stimulation period of 1 to 3 min (Supplementary Fig. 3). As illustrated in Fig. 3a, the attenuation duration significantly increased as the atmospheric temperature decreased, likely due to the greater retention of the shallow trap electrons at lower temperatures than at higher temperatures. Remarkably, the ELD decay time exceeded 600 s at temperatures below 300 K. In consideration of practical applications in low-temperature storage, we employed a storage temperature of 250 K for subsequent characterization of the targeted ELDs. Moreover, the performance of the PersL duration improved with increasing driving AC voltage and tended to saturate at 400 V (Fig. 3b). Notably, while PDMS facilitates powder dispersion and prevents short-circuiting, its effective insulating properties contribute to a PersL turn-on voltage exceeding 100 V. In parallel, elevated frequencies produce a surplus of hot electrons, amplifying the accumulation of electrons within trap states and thereby enhancing the PersL intensity. Nevertheless, the finite nature of the trap density needs to be highlighted since charging saturation was achieved at frequencies greater than 1 kHz (Fig. 3c). Simultaneously, elevated voltage and frequency potentially induce an increase in device temperature, accelerating the release of the charge carriers from traps and consequently minimizing the duration. The total AC waveforms used in Fig. 3b, c have been included in Supplementary Fig. 4. Hence, the AC voltage and frequency were set to 400 V and 1 kHz, respectively, in subsequent experiments. As depicted in Fig. 3d and Supplementary Movie 1, the PersL can be reliably reproduced under the recommended conditions (voltage = 400 V, frequency = 1 kHz, temperature = 250 K) even after undergoing multiple cycles of electrical charging. After charging at 250 K for 300 s, certain charge carriers persisted within the emission layer. Notably, they could be released at a heating rate of 150 K min^{-1} when the temperature is elevated (Fig. 3e and Supplementary Movie 2). These distinct TL signals provided supplementary evidence for the existence of traps with continuous depth distributions. The properties of electrical energy storage and photon release at 250 K are shown in Fig. 3f.

Luminescent center and trap profiles

To gain deeper insights into the luminescent center characteristics, we initially conducted EL spectroscopy at different voltage excitations (Supplementary Fig. 5). The EL intensity was obtained when the voltage exceeded 100 V, with the emission spectrum remaining consistent in the ELD (Fig. 3b and Supplementary Fig. 5). Interestingly, varying frequencies solely impact the color of EL light without exerting any impact on the color of PersL after the AC excitation is ceased (Fig. 3f and Fig. 4a). As documented in numerous studies, the color variation of EL is contingent upon the lifetime of the radiative transitions within the ZnS:Cu phosphor. At elevated frequencies, the EL predominantly consisted of short-lived blue light, whereas at lower frequencies, it primarily comprised long-lived green light (Fig. 2f)[35]. The consistent emission of the AC-charging PersL can be attributed to electrons

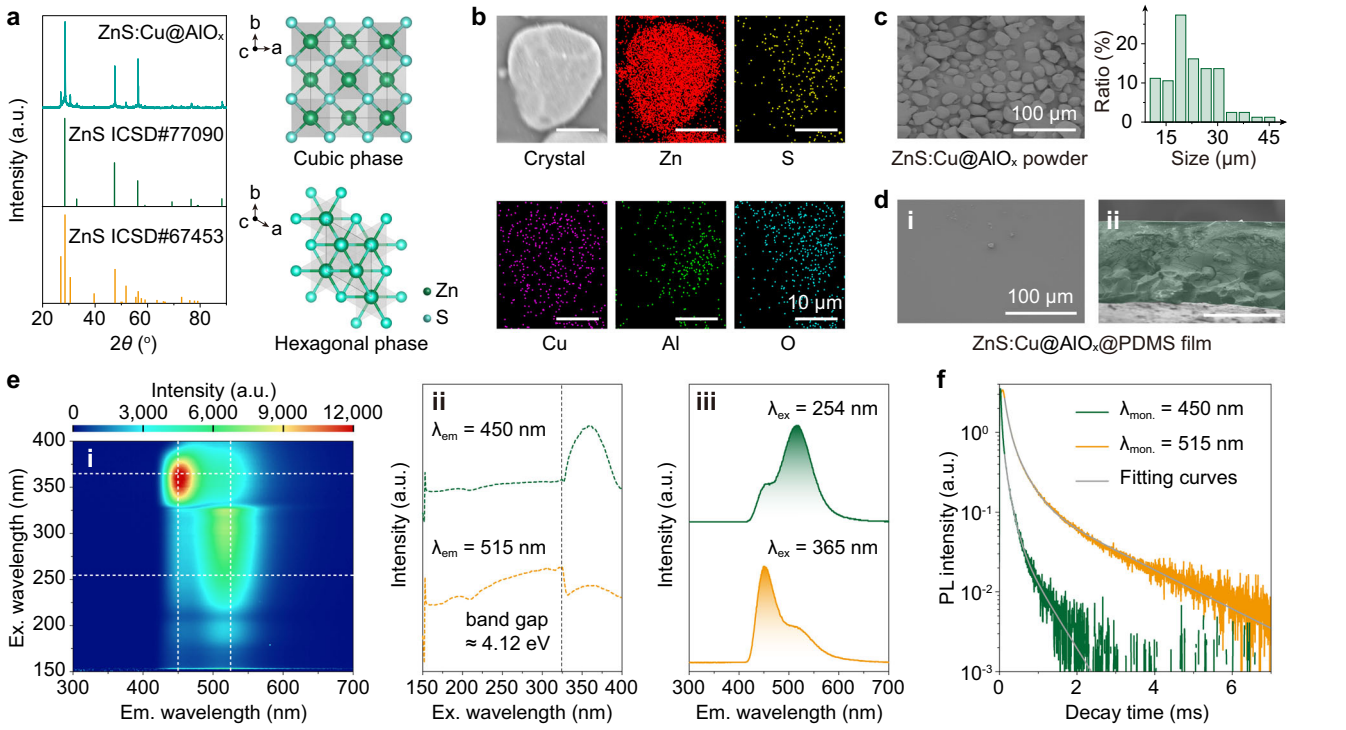

Fig. 2 | Photophysical properties of the ZnS:Cu@AlO$_x$ phosphor. a XRD pattern and crystal structure of ZnS:Cu@AlO$_x$ powder (cubic phase: ICSD#77090 and hexagonal phase: ICSD#67453). **b** Elemental distribution mapping of ZnS:Cu@AlO$_x$ powder. **c** SEM image and particle size distribution of ZnS:Cu@AlO$_x$ powder. **d** Vertical view (i) and front view (ii) of the SEM images of the ZnS:Cu@AlO$_x$@PDMS film (spin-coating speed = 500 rpm). **e** Excitation-emission wavelength 2D contour plot of the PL intensity of ZnS:Cu@AlO$_x$ powder at 10 K and 10^{-7} Pa (i) and corresponding excitation spectra (ii, λ_{em} = 450 and 515 nm) and emission spectra (iii, λ_{ex} = 254 and 365 nm). **f** PL decay curves of the ZnS:Cu@AlO$_x$ powder (λ_{ex} = 300 nm, λ_{em} = 450 nm, and λ_{em} = 515 nm).

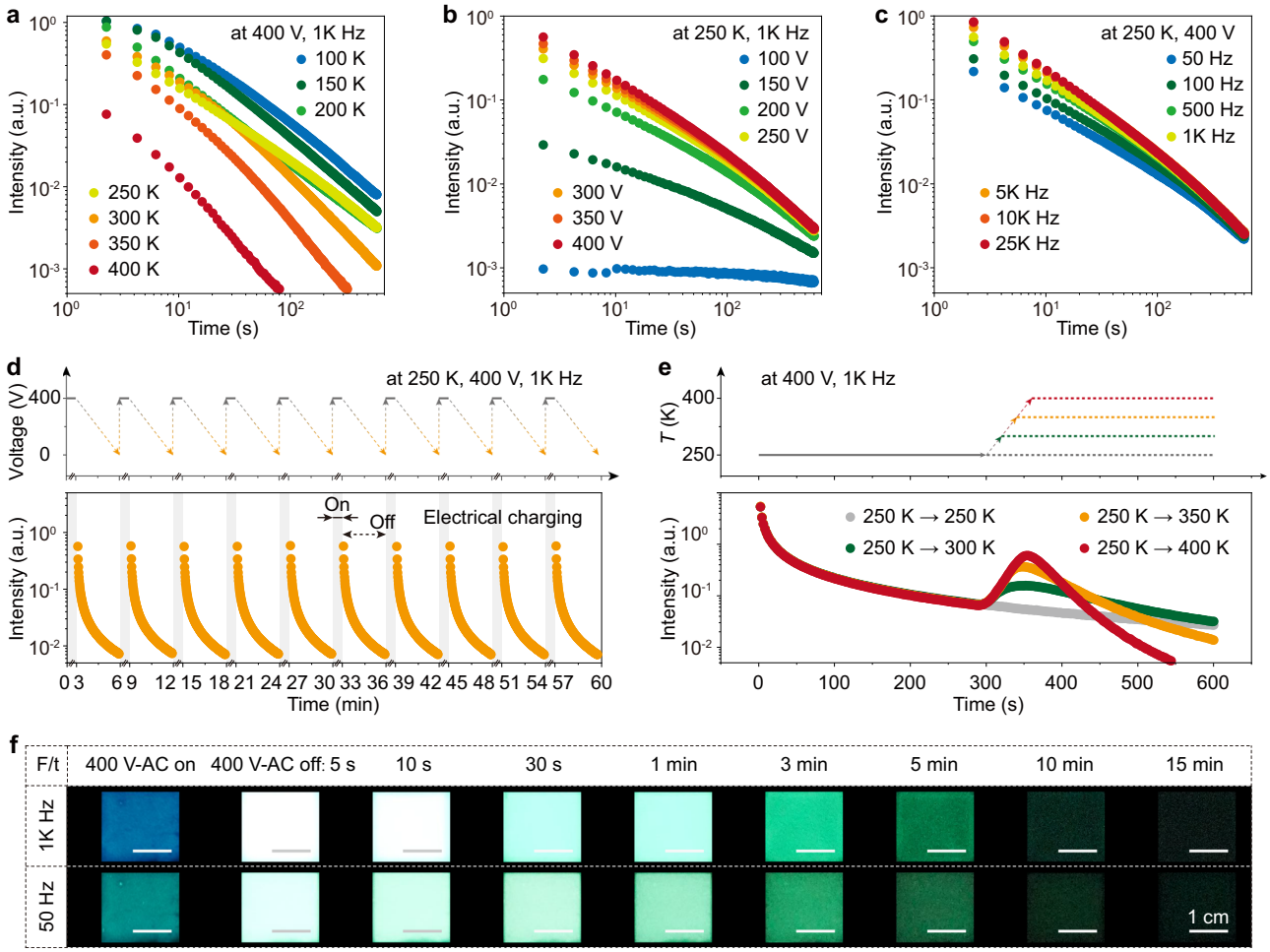

Fig. 3 | Electrically driven PersL properties of the ZnS:Cu@AlO$_x$@PDMS-based ELD. a Temperature-dependent PersL decay curves (setting V = 400 V and F = 1 kHz). **b** Voltage-dependent PersL decay curves (setting T = 250 K and F = 1 kHz). **c** Frequency-dependent PersL decay curves (setting T = 250 K and V = 400 V). **d** Actual voltage profile (top) and 10 repeated PersL decay curves of the ELD after electrical charging (bottom, T = 250 K, V = 400 V, F = 1 kHz, t_{ex} = 3 min, and $t_{mon.}$ = 3 min). **e** Actual temperature profile (top) and PersL decay curve of the ELD (bottom, V = 400 V, F = 1 kHz, t_{ex} = 3 min, and $t_{mon.}$ = 5 min) at 250 K and then heated to 250, 300, 350, and 400 K (heating rate = 150 K min^{-1} and $t_{mon.}$ = 5 min). **f** Photographs of the ELD under AC charging (T = 250 K, V = 400 V, F = 1 kHz and 50 Hz, and t_{ex} = 3 min) and after ceasing electrical charging.

returning from the trap to the luminescent center, resulting in simultaneous dual emissions from the interstitial Cu_i and substitutional Cu_{Zn}, wherein the dominant emission is green light emitted by the latter. We further discovered a temperature-dependent PL spectrum excited at 254 nm that resembled the PersL spectrum following electrical excitation; this featured bimodal emission with predominantly green light peaking at 515 nm (Fig. 4b). This could be attributed to the emission processes originating from the CB or adjacent excited states to the ground state of the luminescent center. Furthermore, TL glow contour mapping at a heating rate of 50 K min^{-1} was obtained after AC charging (Fig. 4c). As the temperature increased from 100 to 450 K, the TL spectra gradually exhibited bimodal emission, characterized by fluctuating intensity while maintaining nearly unshifted peak positions. This pattern also mirrored that of the PL excited by 254 nm UV light, indicating efficient band-to-band separation by hot excitons and charge recombination under thermal stimulation. The short-lived blue light was prone to nonradiative transitions at elevated temperatures, consequently resulting in the material primarily emitting green light at high temperatures.

In a subsequent series of experiments, the TL glow curves were collected at various heating rates (β_h) to compare the trap state characteristics of different kinds of samples under different charging methods. We estimated the trap depth by utilizing the heating rate plot derived from the Randall-Wilkins model[36,37],

$$\frac{\beta_h \cdot \varepsilon}{k_B \cdot T_m^2} = s \cdot \exp\left(\frac{-\varepsilon}{k_B \cdot T_m}\right) \quad (1)$$

where k_B is the Boltzmann constant, T_m (K) is the peak temperature obtained from the TL glow curves, and s (s^{-1}) is the frequency factor. Under 254 nm excitation, the estimated deepest trap depths (ε) decreased with increasing temperature from 285 to 335 K, reaching 0.46 ± 0.01 eV for the ZnS:Cu phosphor, 0.35 ± 0.01 eV for the ZnS:Cu@AlO$_x$ phosphor, and 0.31 ± 0.01 eV for the ZnS:Cu@AlO$_x$@PDMS ELD (Fig. 4d, e and Supplementary Figs. 6-S8). The shallower trap depths likely resulted from the passivation of surface defects, which was particularly evident after coating with the AlO$_x$ shell. A significant shift (> 50 K decrease in T_m) was also observed for the TL peaks at lower temperatures when the TL performance was compared between the pure ZnS:Cu and ZnS:Cu@AlO$_x$ powders under UV excitation (Supplementary Figs 6 and 7). Additionally, further validation confirmed that the traps induced by the PDMS coating became shallower (~10 K) in both the cubic phase and hexagonal phase of the ZnS:Cu powders, as well as in the related phosphor doped into the PDMS films (Supplementary Fig. 9). However, AlO$_x$ and PDMS coatings are essential for enhancing the performance of AC charging PersL and preventing short circuits in devices, respectively. Importantly, depths of approximately

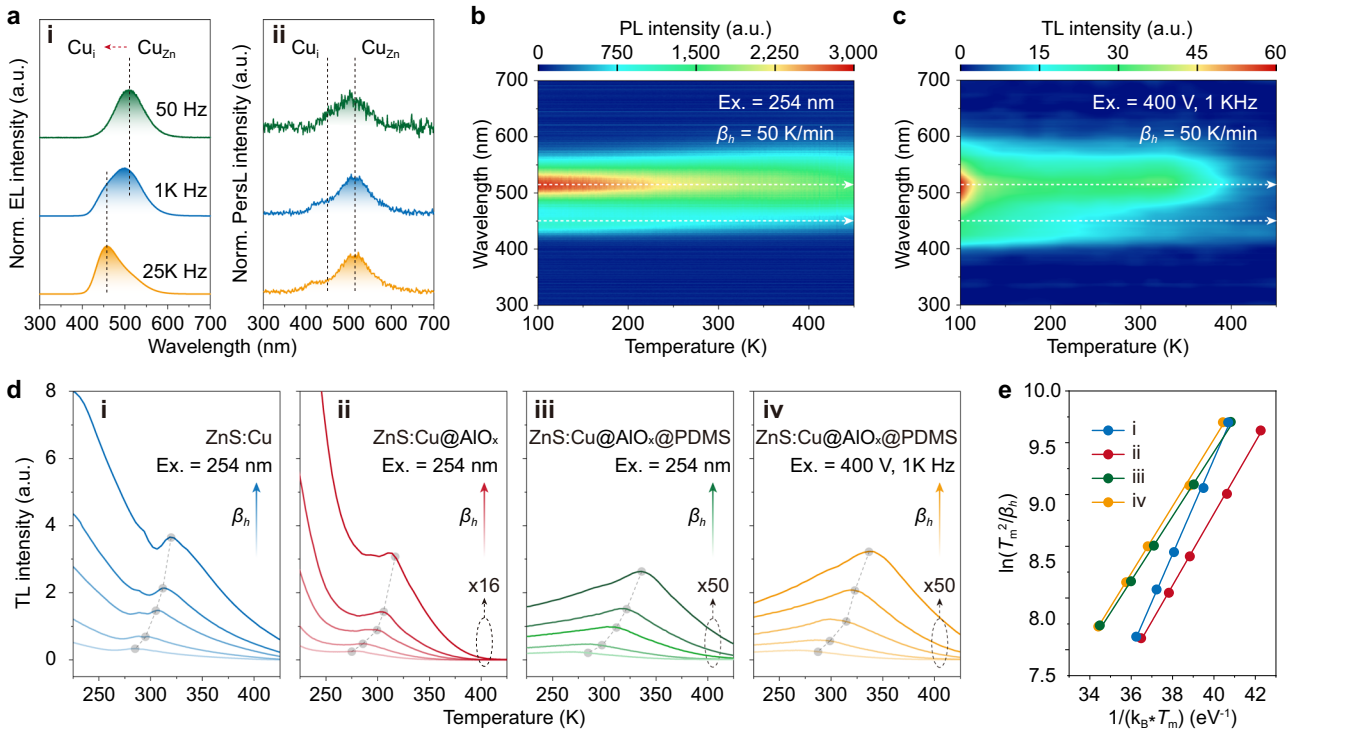

Fig. 4 | Luminescent center and trap profiles of the ZnS:Cu@AlOx@PDMS-based systems. a Normalized EL and PersL of the ZnS:Cu@AlO$_x$@PDMS-based ELD under and after AC charging at various frequencies of 50 Hz, 1 kHz, and 25 kHz (V = 400 V and T = 100 K). **b** PL emission wavelength–temperature contour plots of the ZnS:Cu@AlO$_x$@PDMS film excited with 254 nm UV light. **c**. TL glow contour map of the ZnS:Cu@AlO$_x$@PDMS-based ELD with a heating rate of 50 K min^{-1} after AC charging (V = 400 V, F = 1 kHz, T = 100 K, and t_{ex} = 1 min). **d** TL glow curves of the ZnS:Cu phosphor (i), ZnS:Cu@PDMS film (ii), and ZnS:Cu@PDMS-based ELD under 254 nm excitation (iii, T = 100 K, and t_{ex} = 1 min) and the ZnS:Cu@PDMS-based ELD under AC charging (iv, V = 400 V, F = 1 kHz, T = 100 K, and t_{ex} = 1 min) with different heating rates (5, 10, 20, 30, and 50 K min^{-1}). **e** Estimation of the trap depths of the ZnS:Cu phosphor (i), ZnS:Cu@PDMS film (ii), and ZnS:Cu@PDMS-based ELD under 254 nm excitation (iii) and ZnS:Cu@PDMS-based ELD under AC charging (iv, V = 400 V, F = 1 kHz, T = 100 K, and t_{ex} = 1 min) by using the Randall-Wilkins model.

0.32 ± 0.01 eV were consistently obtained for the ELDs under UV excitation and AC (Fig. 4d iii and iv, Supplementary Fig. 8, and Supplementary Fig. 10). These results indicated that electrical excitation could serve as an effective means of charging trap states. Notably, the initial attenuation observed in the TL curve during temperature elevation (100-150 K) was not attributed to the phosphorescence of the PDMS binder (Supplementary Fig. 11). Rather, this could be ascribed to the coverage of intrinsic defects in the powder, further shifting the main peak temperature of the TL glow curves toward unobservable lower temperatures (Supplementary Fig. 12). Building upon the above results, we propose a mechanism for the electrically driven PersL in ELDs. In the proposed mechanism, during AC charging, electrons in the VB are excited by hot electrons, and the separated charge carriers are subsequently captured by the trap state. During this process, the Cu^+ ions at the luminescent center lose electrons, forming Cu^{2+} ions. The trapped electron will be released with external stimulation. And then the released electron recombine with hole at the luminescent center under Coulomb interaction[38], resulting in Cu^+ ions supported PersL emission with distinct thermal activation characteristics. Notably, the trapped electrons can be stimulated not only by thermal energy but also through electrical energy[39]. The discovery of electrical excitation and stimulation have opened a pathway for the device integration of inorganic PersL materials.

Furthermore, to assess the universality of the proposed approach for AC charging of PersL in inorganic materials, the ZnS:Cu,Al and ZnS:Mn phosphors coated with AlO_x, with particle sizes of approximately 3.7 μm and 6.0 μm, respectively, were selected (Supplementary Figs. 13a, b and Supplementary Figs. 14a, b). Compared to ZnS:Mn@AlO_x phosphors, ZnS:Cu@AlO_x- and ZnS:Cu,Al@AlO_x-based ELDs demonstrate a deeper trap depth (T_m > 300 K with a heating rate of 50 K min^{-1}) after electrical excitation, leading to a longer decay duration and high TL intensity (Supplementary Figs. 13c and Fig. 14c). Notably, the luminescence of this system can be easily regulated by doping different luminescent centers. As depicted in Supplementary Figs. 13d and 14d, the colors of the AC-charging PersL were controllably extended to cyan and orange, with peak wavelengths at 515 nm and 450 nm for ZnS:Cu, Al@AlO_x, and 585 nm for ZnS:Mn@AlO_x, respectively.

Electrical energy storage applications

The time-temperature indicator (TTI) can transform the time-temperature history into easily accessible information, facilitating the monitoring of perishable foods, pharmaceuticals, or specialty chemicals throughout the entire transport-storage process[40]. The liberation of trapped carriers in PersL systems is a kinetic process dependent on thermal activation, and this process exhibits a temperature-time relationship similar to the loss of active ingredients in transporting objects. We developed PersL-type TTI technologies for both inorganic and organic systems using UV light excitation; however, serious concerns remain regarding their photobiological toxicity, photothermal effect, and operational convenience[9,41]. Herein, we first achieved AC charging of PersL TTIs in inorganic systems (Fig. 5a). As shown in Fig. 5b–d, after lowering the atmospheric temperature to 100 K, the film underwent a 3 min AC charging process. Subsequently, the temperature was increased to specific values, and the film was maintained for 3 minutes to replicate the indicator conditions. Finally, the stored electrical energy was released through TL measurements. Notably, the stored energy in the label rapidly dissipates when exposed to temperatures exceeding 300 K ($I_{>300K}$ < 50%I_{100K}). As shown in Fig. 5e, to generate the simulated standard curve for the label maintained at 250 K over various storage times, we initially lowered the atmospheric temperature to 250 K and charged the label at 400 V and 1 kHz for 3 min. Subsequently, the label was maintained

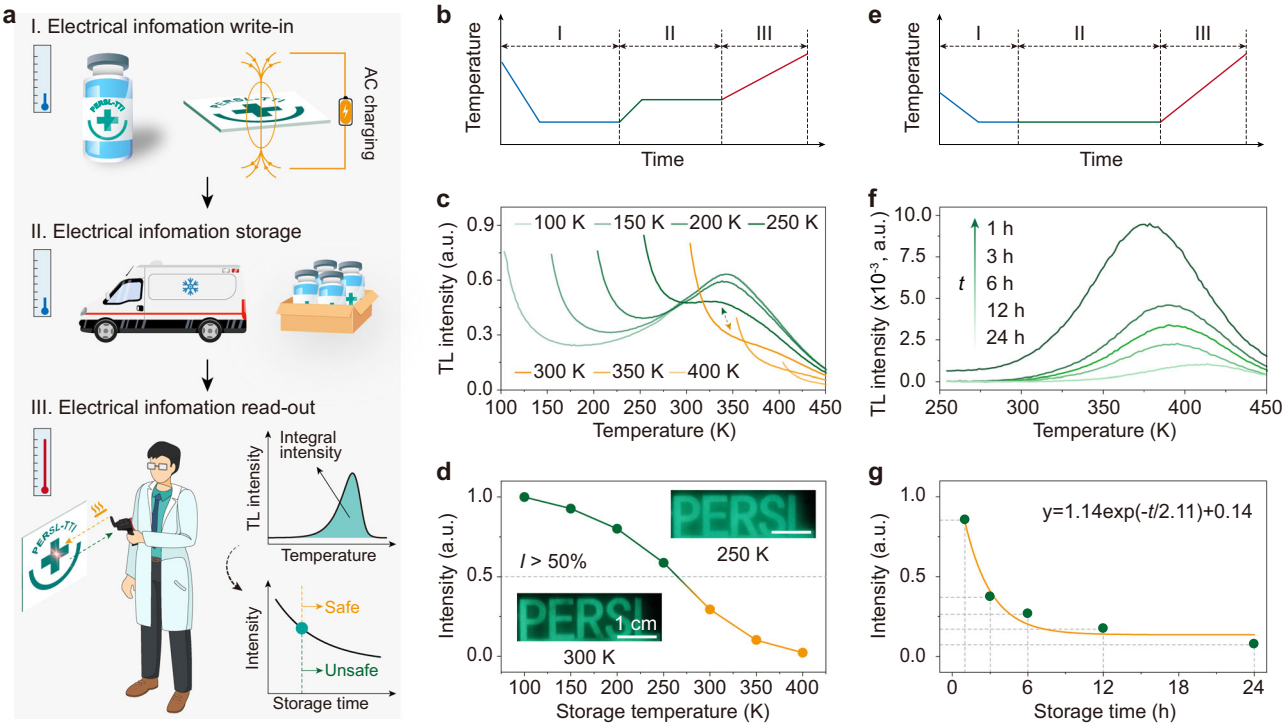

Fig. 5 | Demonstration of a ZnS:Cu@AlOx@PDMS ELD with electrical energy storage properties for TTI applications. a Schematic of PersL TTIs used for electrical information write-in (I), storage (II), and read-out (III) processes. The electrical energy could be stored in the indicator at 250 K after the AC charging is ceased. Then, the medical chemicals are transported to the hospital at a certain time. The energy stored in the label (the integral intensity of the TL spectra) is monitored by heating the label and is then compared to a standard curve to determine whether the medical chemicals have been mutated. **b** Actual temperature profile for different storage temperatures. **c** TL glow curves after being stored at different temperatures (100, 150, 200, 250, 300, 350, and 400 K) for 5 min. **d** Normalized integral intensity of the TL spectrum for each storage temperature. Insert: Photographs of labels charged at 250 and 300 K for 60 s. **e** Actual temperature profile for different storage times. **f** TL glow curves after being maintained at 250 K for different storage times (1, 3, 6, 12, and 24 h). **g** Normalized optical signal intensity as a function of delay time. In the write-in and read-out cycles, the label was irradiated (write-in, I) by AC for 5 min and heated (read-out, III) to 450 K at a heating rate of 50 K min^{-1}.

at 250 K for durations of 1, 3, 6, 12, and 24 h. The stored electrical energy was quantified via the TL measurements, and the standard curve was established by exponentially fitting the integral intensity of the TL spectra. This curve was used to assess the duration and safety of transporting medical items. (Fig. 5f, g).

Conclusions

In conclusion, we propose a versatile methodology to achieve electrically chargeable inorganic PersL with tunable emission wavelengths and trap depths, leveraging conventional AC-driven device architectures. Coating inorganic PersL phosphors with AlO_x and embedding them in PDMS leads to shallower trap depths, while the high dielectric constant of AlO_x and the ultrathin thickness of the EML ensure a uniform electric field distribution during electrical excitation; this facilitates the efficient charge separation at the luminescent center and electron capture at the trap. The trap depths remain consistent at approximately 0.32 ± 0.01 eV after AC charging and light irradiation is ceased; this result indicates that the electric field can function as an alternative excitation source. This work has potential to advance the understanding of inorganic PersL charged with different excitation sources and can extend the applications of inorganic semiconductors in multifunctional photoelectric devices.

Methods

Chemicals and materials

All reagents and chemicals utilized were of reagent grade and commercially available and were used without additional purification. ZnS:Cu (GBF-2F) phosphor was procured from Japan Nemoto & Co., Ltd. ZnS:Cu@AlOx (D502CT), ZnS:Cu,Al (D417S), and ZnS:Mn (D611S) phosphors were sourced from Shanghai Keyan Phosphor Technology Co.,Ltd. Polydimethylsiloxane (PDMS, Dowsil 184) was obtained from Dow Corning. ZnS (99.99%) and NaCl (99%) were purchased from Shanghai Aladdin Biochemical Technology Co., Ltd and $CuCl_2{\cdot}2H_2O$ (AR) was sourced from Xilong Scientific Co., Ltd.

Preparation of ZnS:Cu phosphors

The ZnS and $CuCl_2{\cdot}2H_2O$ were mixed in a molar ratio of 99.99% to 0.01% and placed into a mortar, followed by the addition of anhydrous ethanol for grinding for 45 min. Subsequently, the mixed powder was transferred to an alumina crucible, and a mass of NaCl equal to 1.5 times the mass of the mixed powder was added. The crucible was then placed in a muffle furnace and sintered at 900 °C (cubic phase)/1050 °C (hexagonal phase) for 3 h. After cooling, the samples were washed and dried to obtain the pure ZnS:Cu powder.

Preparation of ELD

The PersL phosphors were blended with PDMS to form the emission layer of the ELD. The weight ratios of the PersL phosphors to the PDMS precursors (including curing agents) were maintained at 1:1. The ratios of the precursors to the corresponding curing agents for PDMS were 10:1 by weight. After vigorous stirring, the mixtures were vacuumed in an oven for 10 min to eliminate air bubbles. Subsequently, the bubble-free mixture was coated into a thin film using the spin coating method (with speeds ranging from 500 to 6000 rpm). The spin-coated film was then dried at 80 °C for 2 h. Following this, a conductive silver paste was applied onto the emission layer using a scraping method and dried at 80 °C for 30 min. To facilitate testing, copper foil or carbon cloth was attached to the upper layer of the silver electrode.

Characterizations of photophysical properties

The XRD patterns of the phosphors were captured utilizing a Bruker D8 Advance X-ray diffractometer, employing Cu Kα radiation (λ = 0.15406 nm) at 40 kV and 40 mA. Surface morphology and elemental mapping were conducted using a field emission scanning electron microscopy (SU70, Hitachi) instrument, which was equipped with EDX spectroscopy. VUV spectroscopy in ZnS:Cu@AlO_x at 10 K was conducted using the beamline BL3B at the UVSOR facility (Institute for Molecular Science, Okazaki, 24IMS6020). Transient decay curve was collected in a fluorescence spectrometer (Acton SP 2300i, Princeton Instruments). Temperature-dependent PL spectra were obtained using customized measurement equipment. The sample was excited with a 254 nm optical parametric oscillator laser (NT342B-20-SH/SF, Ekspla) and initially cooled to 100 K before being heated to 450 K at a predefined rate of 2 K min^{-1}, with the emission intensity recorded in real-time a CCD detector (Roper Scientific, LN/CCD-100EB-GI). Photographs and videos of the samples were taken with a digital camera (α7SIII, SONY).

Characterizations of PersL and TL

The PersL decay curve and TL glow curve spectra were recorded using a custom-built measurement system. Initially, samples were positioned on a cooling-heating stage (THMS600E, Linkam Scientific Instruments) capable of maintaining temperatures from 100 to 600 K. The sample chamber was purged with dry nitrogen gas, and a quartz glass cover was fitted on top. For excitation, samples were either subjected to a specific voltage (for ELDs) using waveform generators (DG821, RIGOL) and high voltage amplifier (HA-820, PINTECH) or exposed to ultraviolet light through the quartz glass (for films) at an excitation power density of approximately 5 mW cm^{-2} for 1 min. Monitoring of PersL intensity (or PersL decay profiles and TL emission) after excitation cessation was accomplished using a filter-attached photomultiplier tube (PMT, R928P, Hamamatsu photonics), a multimeter (2400, KEITHLEY), and a high-voltage power supply (HVC1800, ZOLIX). Simultaneously, PersL spectra were captured using a multichannel spectrometer (QE-Pro, Ocean Photonics) during TL measurements. In a typical TL measurement, the sample was initially cooled to 100 K and stimulated by the excitation sources for 1 min. After a 20 s delay following excitation cessation, the sample was heated to 450 K at a predefined heating rate (5, 10, 20, 30, or 50 K min^{-1}), and emission intensity was recorded in real-time. The entire measurement system was controlled by LabVIEW-based computer programs. And a TL glow curve starting from 10 K was measured using a custom-built setup, which included a cryostat (VPF-800, Janis), an excitation source consisting of a Xe lamp with a cold mirror (LAX-101, Asahi spectra), and a detector composed of a PMT covered by a longpass filter (FELH0450, Thorlabs).

Preparation of TTI label

We customized patterned ITO glass (P-E-R-S-L) and spin-coated the ZnS@AlO_x@PDMS emission layer and cathode materials onto the patterned ITO, enabling the patterning of the TTI labels.

Data availability

Source data are provided with this paper. The remaining data supporting the findings of this study are available within the paper and its Supplementary Information files, and are available from the corresponding author upon reasonable request. The data of Figs. 2–5 have been deposited as a dataset in the Figshare (https://doi.org/10.6084/m9.figshare.28190303).

Received: 26 November 2024; Accepted: 22 January 2025;
Published online: 05 February 2025

References

1. Yamamoto, H. & Matsuzawa, T. Mechanism of long phosphorescence of $SrAl_2O_4$:Eu^{2+}, Dy^{3+} and $CaAl_2O_4$:Eu^{2+}, Nd^{3+}. *J. Lumines.* **72-74**, 287–289 (1997).
2. Li, Y., Gecevicius, M. & Qiu, J. Long persistent phosphors-from fundamentals to applications. *Chem. Soc. Rev.* **45**, 2090–2136 (2016).
3. Ou, X. et al. High-resolution X-ray luminescence extension imaging. *Nature* **590**, 410–415 (2021).
4. Maldiney, T. et al. The in vivo activation of persistent nanophosphors for optical imaging of vascularization, tumours and grafted cells. *Nat. Mater.* **13**, 418–426 (2014).
5. Miao, Q. et al. Molecular afterglow imaging with bright, biodegradable polymer nanoparticles. *Nat. Biotechnol.* **35**, 1102–1110 (2017).
6. Chun, F. et al. Multicolour stretchable perovskite electroluminescent devices for user-interactive displays. *Nat. Photon*. **18**, 856–863 (2024)
7. Xu, J. & Tanabe, S. Persistent luminescence instead of phosphorescence: History, mechanism, and perspective. *J. Lumines.* **205**, 581–620 (2019).
8. Kobe, R. & Adachi, C. Organic long persistent luminescence. *Nature* **550**, 384–387 (2017).
9. Lin, C. et al. Charge trapping for controllable persistent luminescence in organics. *Nat. Photon.* **18**, 350–356 (2024).
10. Lin, C. et al. Enabling Visible-light-charged near-infrared persistent luminescence in organics by intermolecular charge transfer. *Adv. Mater*. e2401000 (2024).
11. Ueda, J., Miyano, S. & Tanabe, S. Formation of deep electron traps by Yb^{3+} codoping leads to super-long persistent luminescence in Ce^{3+}-doped yttrium aluminum gallium garnet phosphors. *ACS Appl. Mater. Interf.* **10**, 20652–20660 (2018).
12. Liang, L. et al. Controlling persistent luminescence in nanocrystalline phosphors. *Nat. Mater.* **22**, 289–304 (2023).
13. Zhao, W., He, Z. & Tang, B. Z. Room-temperature phosphorescence from organic aggregates. *Nat. Rev. Mater.* **5**, 869–885 (2020).
14. Lin, H. et al. Bandgap tailoring via Si doping in inverse-garnet $Mg_3Y_2Ge_3O_{12}$:Ce^{3+} persistent phosphor potentially applicable in AC-LED. *ACS Appl. Mater. Interf.* **7**, 21835–21843 (2015).
15. Lv, H. et al. Highly stable metal-free long-persistent luminescent copolymer for low flicker AC-LEDs. *Angew. Chem. Int. Ed.* **61**, e202204209 (2022).
16. Kabe, R., Notsuka, N., Yoshida, K. & Adachi, C. Afterglow organic light-emitting diode. *Adv. Mater.* **28**, 655–660 (2016).
17. Tan, S., Jinnai, K., Kabe, R. & Adachi, C. Long-persistent luminescence from an exciplex-based organic light-emitting diode. *Adv. Mater.* **33**, 2008844 (2021).
18. Qiu, W. et al. Afterglow OLEDs incorporating bright closely stacked molecular dimers with ultra-long thermally activated delayed fluorescence. *Matter* **6**, 1231–1248 (2023).
19. Feng, H.-T. et al. Tuning molecular emission of organic emitters from fluorescence to phosphorescence through push-pull electronic effects. *Nat. Commun.* **11**, 2617 (2020).
20. Yu, Y. et al. Small-molecule-based organic field-effect transistor for nonvolatile memory and artificial synapse. *Adv. Funct. Mater.* **29**, 1904602 (2019).
21. Peng, J. et al. Atomically resolved single-molecule triplet quenching. *Science* **373**, 452–456 (2021).
22. Wang, L., Xiao, L., Gu, H. & Sun, H. Advances in alternating current electroluminescent devices. *Adv. Optical Mater.* **7**, 1801154 (2019).
23. Douglas, A. A. et al. Hot electron luminescence in ZnS alternating-current thin-film electroluminescent devices. *Appl. Phys. Lett.* **63**, 231–233 (1993).
24. Zhuang, Y. et al. Visualizing dynamic mechanical actions with high sensitivity and high resolution by near-distance mechanoluminescence imaging. *Adv. Mater.* **34**, 2202864 (2022).
25. Lee, G. et al. Interfacial triboelectricity lights up phosphor-polymer elastic composites: unraveling the mechanism of mechanoluminescence in zinc sulfide microparticle-embedded polydimethylsiloxane films. *Small* **20**, 2307089 (2024).

26. Dorenbos, P. Determining binding energies of valence-band electrons in insulators and semiconductors via lanthanide spectroscopy. *Phys. Rev. B* **87**, 035118 (2013).
27. Arbell, H. & Halperin, A. Thermoluminescence of ZnS single crystals. *Phys. Rev.* **117**, 45–52 (1960).
28. Peng, W. Q., Cong, G. W., Qu, S. C. & Wang, Z. G. Synthesis and photoluminescence of ZnS:Cu nanoparticles. *Optical Mater* **29**, 313–317 (2006).
29. Kawashima, S. Blue and green luminescence centers of electroluminescent ZnS:Cu phosphors. *Jpn. J. Appl. Phys.* **5**, 1161 (1966).
30. Clabau, F. et al. Formulation of phosphorescence mechanisms in inorganic solids based on a new model of defect conglomeration. *Chem. Mater.* **18**, 3212–3220 (2006).
31. Lin, K. B. & Su, Y. H. Photoluminescence of Cu:ZnS, Ag:ZnS, and Au:ZnS nanoparticles applied in bio-LED. *Appl. Phys. B* **113**, 351–359 (2013).
32. Shin, S. W. et al. Origin of mechanoluminescence from Cu-doped ZnS particles embedded in an elastomer film and its application in flexible electro-mechanoluminescent lighting devices. *ACS Appl. Mater. Interf.* **8**, 1098–1103 (2016).
33. Urabe, K., Shionoya, S. & Suzuki, A. Polarization of the blue-copper luminescence in ZnS crystals. *J. Phys. Soc. Jpn.* **25**, 1611–1617 (1968).
34. Nien, Y.-T. & Chen, I.-G. Raman scattering and electroluminescence of ZnS:Cu,Cl phosphor powder. *Appl. Phys. Lett.* **89**, 261906 (2006).
35. Jeong, S. M., Song, S. & Kim, H. Simultaneous dual-channel blue/green emission from electro-mechanically powered elastomeric zinc sulphide composite. *Nano Energy* **21**, 154–161 (2016).
36. Bos, A. J. J. Thermoluminescence as a research tool to investigate luminescence mechanisms. *Materials* **10**, 1357 (2017).
37. Zhou, X. et al. Energy-trapping management in x-ray storage phosphors for flexible 3D imaging. *Adv. Mater.* **35**, 2212022 (2023).
38. Chen, J. et al. Tenfold enhancement in light emission from low-temperature operational doped oleds by detrapping super-long-lived trapped charges. *Adv. Funct. Mater.* **33**, 2305560 (2023).
39. Ma, X., Wang, Y. & Seto, T. Electrical stimulation for brighter persistent luminescence. *Light Sci. Appl.* **13**, 165 (2024).
40. McMinn, W. A. M. & Magee, T. R. A. Kinetics of ascorbic acid degradation and non-enzymic browning in potatoes. *Food Bioprod. Process.* **75**, 223–231 (1997).
41. Song, Y. et al. Recyclable time-temperature indicator enabled by light storage in particles. *Adv. Optical Mater.* **11**, 2202654 (2023).

Acknowledgements

This research is financially supported by JSPS KAKENHI (grant number 24K01581, 20H02438), the Joint Studies Program of the Institute for Molecular Science (24IMS6020), the National Natural Science Foundation of China (52102175, 52202194), the Fundamental Research Funds for the Central Universities (2682024CX098), the New Interdisciplinary Cultivation Funds of Southwest Jiaotong University (2682024KJ002).

Author contributions

C.L. and R.Y. contributed equally to this work. C.L., R.Y., S.Y., Y.L. and J.U. conceived the experiments. C.L., R.Y., S.Y., Y.L., YX.Z., R.-J.X. and J.U. prepared the paper. C.L., R.Y., Z.W., Y.W., C.Z., H.M., X.Z., YT.Z., S.Y., Y.L. and J.U. were primarily responsible for the experiments. All authors contributed to the data analyses.

Competing interests

The authors declare no competing interests.

Additional information

Supplementary information The online version contains supplementary material available at https://doi.org/10.1038/s43246-025-00746-x.

Correspondence and requests for materials should be addressed to Shihai You, Ying Lv or Jumpei Ueda.

Peer review information *Communications Materials* thanks Jing Chen and the other, anonymous, reviewer(s) for their contribution to the peer review of this work. Primary Handling Editors: Jet-Sing Lee. A peer review file is available.

Reprints and permissions information is available at http://www.nature.com/reprints

Publisher's note Springer Nature remains neutral with regard to jurisdictional claims in published maps and institutional affiliations.

Open Access This article is licensed under a Creative Commons Attribution-NonCommercial-NoDerivatives 4.0 International License, which permits any non-commercial use, sharing, distribution and reproduction in any medium or format, as long as you give appropriate credit to the original author(s) and the source, provide a link to the Creative Commons licence, and indicate if you modified the licensed material. You do not have permission under this licence to share adapted material derived from this article or parts of it. The images or other third party material in this article are included in the article's Creative Commons licence, unless indicated otherwise in a credit line to the material. If material is not included in the article's Creative Commons licence and your intended use is not permitted by statutory regulation or exceeds the permitted use, you will need to obtain permission directly from the copyright holder. To view a copy of this licence, visit http://creativecommons.org/licenses/by-nc-nd/4.0/.

© The Author(s) 2025